IOP Publishing Nanotechnology

Nanotechnology **30** (2019) 135701 (10pp) https://doi.org/10.1088/1361-6528/aafc85

Structural characterization of bulk and nanoparticle lead halide perovskite thin films by (S)TEM techniques

N Fernández-Delgado[1], M Herrera[1], F J Delgado[1], A H Tavabi[2], M Luysberg[2], R E Dunin-Borkowski[2], E J Juárez-Pérez[3], B Clasen Hames[3], I Mora-Sero[3], I Suárez[4], J P Martínez-Pastor[4] and S I Molina[1]

[1] Department of Material Science, Metallurgical Engineering and Inorganic Chemistry IMEYMAT, University of Cadiz, Spain
[2] Ernst Ruska-Centre for Microscopy and Spectroscopy with Electrons and Peter Grünberg Institute, Forschungszentrum Jülich, Germany
[3] Institute of Advanced Materials (INAM), University of Jaume I, Spain
[4] Research Institute of Materials Science, University of Valencia, Spain

E-mail: natalia.fernandezdelgado@uca.es

Received 26 October 2018, revised 22 December 2018
Accepted for publication 8 January 2019
Published 4 February 2019

Abstract

Lead halide ($APbX_3$) perovskites, in polycrystalline thin films but also perovskite nanoparticles (NPs) has demonstrated excellent performance to implement a new generation of photovoltaic and photonic devices. The structural characterization of $APbX_3$ thin films using (scanning) transmission electron microscopy ((S)TEM) techniques can provide valuable information that can be used to understand and model their optoelectronic performance and device properties. However, since $APbX_3$ perovskites are soft materials, their characterization using (S)TEM is challenging. Here, we study and compare the structural properties of two different metal halide $APbX_3$ perovskite thin films: bulk $CH_3NH_3PbI_3$ prepared by spin-coating of the precursors in solution and $CsPbBr_3$ colloidal NPs synthetized and deposited by doctor blading. Both specimen preparation methods and working conditions for analysis by (S)TEM are properly optimized. We show that $CH_3NH_3PbI_3$ thin films grown by a one-step method are composed of independent grains with random orientations. The growth method results in the formation of tetragonal perovskite thin films with good adherence to an underlying TiO_2 layer, which is characterized by a photoluminescence (PL) emission band centered at 775 nm. The perovskite thin films based on $CsPbBr_3$ colloidal NPs, which are used as the building blocks of the film, are preserved by the deposition process, even if small gaps are observed between adjacent NPs. The crystal structure of $CsPbBr_3$ NPs is cubic, which is beneficial for optical properties due to its optimal band gap. The absorption and PL spectra measured in both the thin film and the colloidal solution of $CsPbBr_3$ NPs are very similar, indicating a good homogeneity of the thin films and the absence of aggregation of NPs. However, a particular care was required to avoid long electron irradiation times during our structural studies, even at a low voltage of 80 kV, as the material was observed to decompose through Pb segregation.

Keywords: lead halide perovskites, HRTEM, EDX

(Some figures may appear in colour only in the online journal)

Introduction

Lead halide (APbX3) perovskites are highly promising materials for optoelectronic and photonic devices. In fact, these materials have been widely used in solar cell [1–3], light-emitting diode [4–5] and lasing [6–7], because of their high photo-conversion efficiencies (up to 22.7%), excellent light emission properties [8], and low cost fabrication [1]. Their outstanding properties include high absorption coefficients and sharp absorption edges [9], band gaps that are tunable with composition, and high emission quantum yields at room temperature. Hybrid $CH_3NH_3PbI_3$ has attracted particular attention, as it is the first lead halide perovskite used in photovoltaic applications [9–10]. $CH_3NH_3PbI_3$ semiconductor has a direct band gap of ∼1.6 eV and high carrier mobility, resulting in solar cells with conversion efficiencies of up to 22.7% [11], and optical amplifiers with low thresholds of stimulated emission [12]. However, $CH_3NH_3PbI_3$ films degrade under ambient conditions, especially in the presence of moisture [13–14]. In contrast, inorganic perovskites have demonstrated higher stability [15–16]. In particular, $CsPbBr_3$ nanocrystals have been shown to exhibit ∼90% photoluminescence (PL) efficiency with a narrow full width at half maximum (FWHM) [17–18] and have a highly emissive crystal phase that is stable at room temperature [19], leading to enormous potential for applications in optoelectronic devices. Examples of inorganic perovskite-based devices are light-emitting diodes [20], photodetectors [21] and solar cells [22].

Although both bulk and nanoparticle (NP) thin films have similar perovskite lattices, they have different structural properties that need to be understood to optimize their optoelectronic properties and to integrate them efficiently in solid state devices. Control of their structural properties, such as crystallinity [23] and composition [24], is a key issue for device efficiency. Crystalline defects and grain boundaries can act as non-radiative recombination sites that affect photovoltaic properties [25–26]. Parameters such as film roughness and surface coverage after deposition of the material on a substrate also need to be controlled to obtain smooth and continuous layers in high-efficiency solar cells [27–28]. Other issues include the long-term stability of the active layer. The coverage of the perovskite with polymeric materials is one of the most common solutions to improve the stability of the perovskites. Thus, polymers such as poly(methyl methacrylate) (PMMA), polyvinyl alcohol or poly vinylpyrrolidone have been considered. Among them, PMMA has shown to provide larger air stability to the perovskite [29]. FTIR has shown that this could be due to the interaction between the carbonyl groups of PMMA and the Pb cations of the lead halide perovskite [30]. Additionally, the PMMA coverage also benefits the propagation of the excitation beam along the semiconductor [12].

Detailed information about the structural properties of the material after deposition on a substrate is therefore essential. However, only indirect measurements are typically used. For example, the defect density in $CH_3NH_3PbI_3$ perovskites has been quantified using first-principles calculations and spectroscopic measurements [31]. Direct measurements of the structural properties of $APbX_3$ perovskites are required to understand and improve synthesis, deposition processes and the influence of the A cation component in the electronic band structure and the subsequent optical and optoelectronic properties. For this purpose, transmission electron microscopy (TEM) and (scanning) transmission electron microscopy ((S)TEM) are powerful techniques for the local microstructural characterization of advanced materials [32–33]. Crystalline structure [34] and iodide migration [35] have been studied in $CH_3NH_3PbI_3$ perovskites using these techniques. Furthermore, they have been used to identify new phases in $CsPbBr_3$ NPs, such as $CsPb_2Br_5$ during the synthesis of $CsPbBr_3$ [36]. Although these studies demonstrate their benefit for the knowledge advance of perovskite materials, the characterization of lead halide perovskites by (S)TEM techniques presents particular challenges, as the incident electron beam can degrade the material. As this previous examples highlight, (S)TEM characterization of perovskites is not straightforward neither in standard layers nor in films formed by NPs, here we report, as far as we know, the first comparative study of these two important families of perovskite materials.

We analyze the structural properties of two different perovskite thin films, comprising bulk $CH_3NH_3PbI_3$ and $CsPbBr_3$ NPs, using (S)TEM techniques. Both films were deposited on SiO_2/TiO_2 substrates, in order to ensure an easy cleavage, and covered by PMMA to enhance their stability to ambient conditions. Specimen preparation and imaging conditions for electron microscopy were optimized to avoid degradation of the materials during the measurements. Special attention was paid to understand the morphologies of the layers and their crystal structures. For this purpose, (S)TEM characterization of both kinds of perovskite thin films was properly compared in order to understand the influence of the composition and nature of the base material (chemical precursors or colloidal NPs) in the crystal structure and morphology of the resulting film. Since these parameters affect the functionalities of potential optoelectronic devices, we believe that this characterization could be beneficial in the implementation of future perovskite-based devices.

Materials and methods

Bulk $CH_3NH_3PbI_3$ perovskite thin film preparation

Si/SiO_2 wafers were cleaned sequentially using acetone, ethanol and isopropanol. The wafers were dried using a N_2 stream and heated for 1 min at 100 °C over a hot plate. A ∼40 nm thick layer of TiO_2 was deposited on the Si/SiO_2 wafer by spin-coating an anhydrous ethanol solution of titanium isopropoxide and heating at 500 °C for 30 min in room atmospheric conditions. The lead halide perovskite layer was deposited in a glove-box by spin-coating 100 μl of the perovskite precursor DMF solution of 40% or 10% (w/w) onto the wafer. After deposition, the substrate was kept at room temperature for 15 min and then heated to 100 °C for 1 h in an oven in air. After depositing the perovskite onto the substrate,

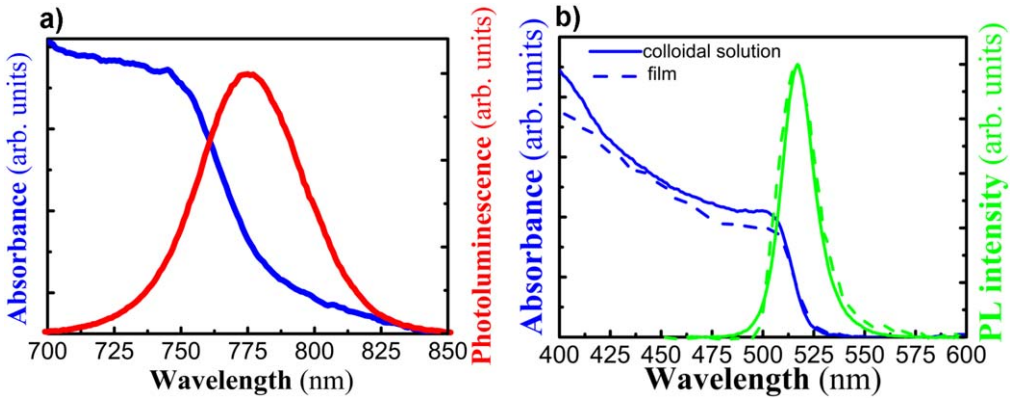

Figure 1. (a) Absorbance and PL spectra recorded from the $CH_3NH_3PbI_3$ film; (b) absorbance and PL spectra recorded from $CsPbBr_3$ nanoparticles (NPs) in colloidal solution and a film.

a solution of PMMA in toluene was spin coated onto the sample and heated at 150 °C.

$CsPbBr_3$ NP synthesis and sample deposition

In order to synthesize $CsPbBr_3$ NPs, $PbBr_2$ (0.4 mmol) and CsBr (0.4 mmol) were dissolved in DMF (10 ml). Upon complete dissolution of the precursors, oleic acid (1.0 ml) and oleylamine (0.5 ml) were added to stabilize the precursor solution. Then, the precursor solution (1.0 ml) was added dropwise to toluene (10 ml) under vigorous stirring. Strong green emission was observed immediately after injection [18]. Thin films of $CsPbBr_3$ NPs were prepared from the colloidal solution using a doctor blading technique. This deposition method ensures good film homogeneity and avoids agglomeration of the NPs, as we demonstrated previously for colloidal NPs [37].

Characterization

PL measurements were performed in backscattering geometry using a continuous wave excitation laser at 404 nm under a weak pump fluency of 20 W cm^{-2} and collecting the back-emitted PL into an HR4000 Ocean Optics spectrograph.

Absorption was obtained using a Shimadzu UV-2501PC spectrophotometer (UV–visible range), or by measuring the transmittance using a commercial reflectometer (Nanocalc from Micropack).

Electron-transparent specimens of $CH_3NH_3PbI_3$ were prepared for (S)TEM analysis using two methods. The first method involved conventional grinding, polishing and Ar^+ ion milling using a precision ion polishing system (PIPS) from Gatan. The second method involved focused ion beam (FIB) milling using a Helios Nanolab 650 DualBeam from FEI Company. The $CsPbBr_3$ specimen was also prepared using FIB milling. (S)TEM measurements were performed using an FEI Titan Themis Cubed TEM and an FEI Titan G2 80–200 ChemiSTEM equipped with a Super-X energy dispersive x-ray (EDX) spectrometer. Eje Z software [38] was used for the simulation of digital diffraction patterns (DDPs) of the perovskites. The $CH_3NH_3PbI_3$ perovskites considered are orthorhombic (*Pnma*), tetragonal (*I4/mcm*) and cubic (*Pm3m*), while the $CsPbBr_3$ perovskites considered are cubic (*Pm3m*), tetragonal (*P4/mbm*) and orthorhombic (*Pnma*).

Results and discussion

Figure 1(a) shows absorbance and PL spectra recorded from the $CH_3NH_3PbI_3$ perovskite film as blue and red lines, respectively. The sharp absorption edge is localized at 750–760 nm, while the exciton absorption peak is centered at 750 nm, in accordance with previous publications [9]. The PL emission band has a Gaussian shape centered on 775 nm which is associated with a tetragonal structure [39], and has a FWHM of 46 nm. The absorption of colloidal $CsPbBr_3$ NPs in this work (solid blue line in figure 1(b)) is associated with a band edge at ∼510 nm, with the excitonic peak localized at 501 nm, in agreement with previous results reported for this material [40]. The PL spectrum has a Gaussian shape (green solid line in figure 1(b)), which is centered at 517 nm, is related to the cubic structure [41] and has a FWHM of 21 nm. This red Stokes shift can be explained by aggregation of the NPs [42]. The film of colloidal NPs shows similar absorption and PL as the colloidal solution (blue and green dashed lines in figure 1(b), respectively), indicating good homogeneity and the absence of aggregation of NPs in the film.

TEM analysis of $CH_3NH_3PbI_3$ initially focused on the specimen prepared using a conventional method. Figure 2(a) shows a TEM image, in which the different layers of the structure can be distinguished. In order to study the crystalline quality of the layers, fast Fourier transform (FFT) analysis was carried out. Surprisingly, most of the material formed on the TiO_2 layer was found to be non-crystalline, as shown by characteristic amorphous rings in the corresponding FFT (see inset to figure 2(a)). EDX analysis shows that the composition of the amorphous material is consistent with that expected for the perovskite layer, as shown in the second inset to figure 2(a). The large amount of amorphous material present suggests that amorphization may have taken place during specimen preparation for TEM. FIB milling was therefore used as an alternative specimen preparation procedure. Figure 2(b) shows a TEM image of $CH_3NH_3PbI_3$ prepared

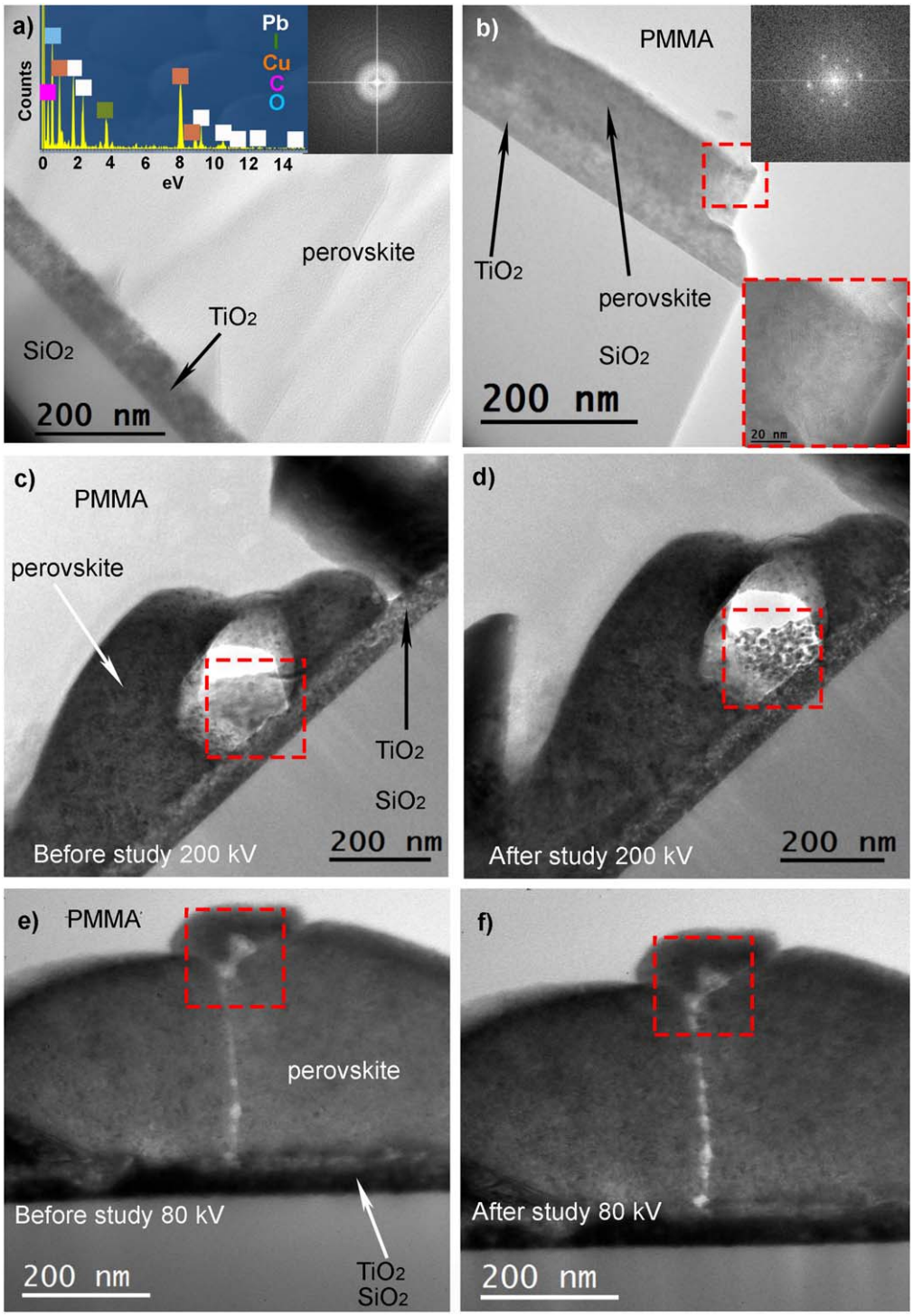

Figure 2. (a) and (b) TEM images of $SiO_2/TiO_2/CH_3NH_3PbI_3$ specimens prepared (a) by conventional milling and (b) by FIB milling. (c)–(f) TEM images of the sample prepared by FIB milling recorded (c), (d) and (e) before, (f) after electron irradiation at (c), (d) and (e) 200, (f) 80 kV.

using FIB milling, in which the perovskite and TiO_2 layers can now be observed. The FFT (shown as an inset) contains spots corresponding to a crystalline structure. A second inset shows a high-resolution TEM (HRTEM) image of $CH_3NH_3PbI_3$, in which atomic planes can be distinguished, confirming the crystalline nature of the material. The advantage of FIB milling for preparation of halide perovskites for (S)TEM results from the use of a Ga^+ ion gun with a well-controlled beam to thin the specimen to electron transparency. The angle of incidence of the Ga^+ ions is almost parallel to the surface of the material during thinning, whereas in the PIPS used for conventional preparation the Ar^+ ion beam has an angle of 3.5°. Although the same ion voltage (~2 kV) is used in the last step of the thinning process in both methods,

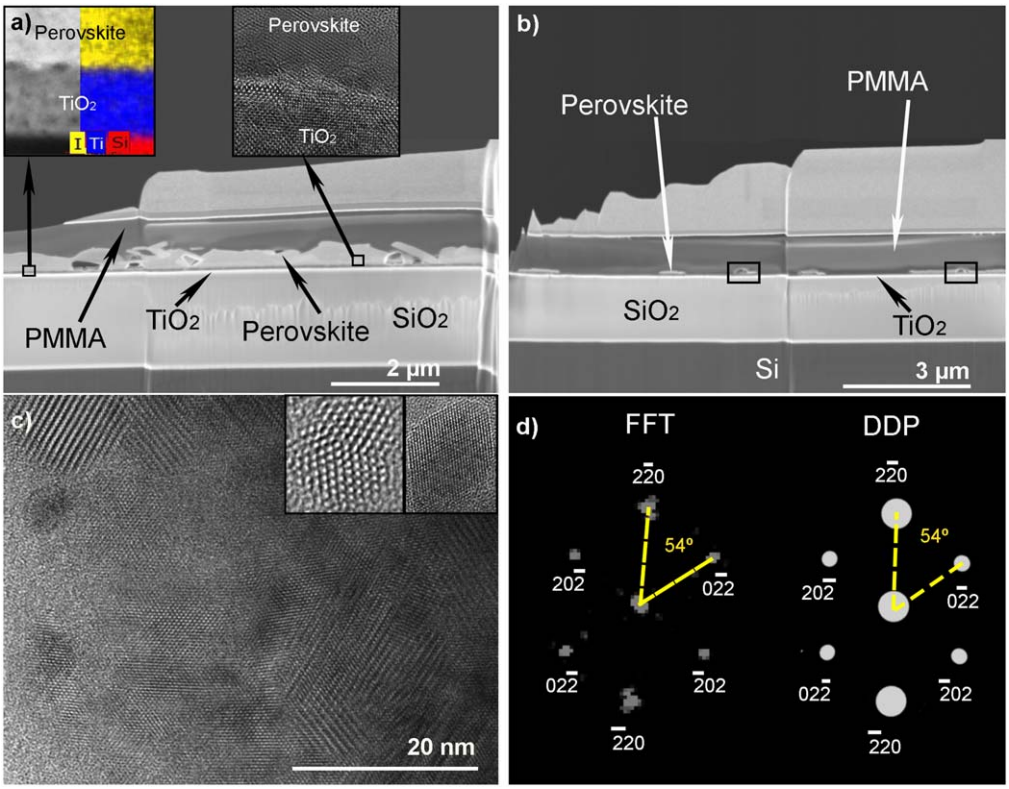

Figure 3. SEM images of CH3NH3PbI3 lamella for (a) 40% and (b) 10% (w/w) concentrations of the precursor samples. (c) HRTEM image of the CH3NH3PbI3 region, with the inset showing faceted particles. (d) Experimental FFT shown alongside a calculated DDP for a tetragonal crystal structure.

the PIPS is more aggressive than the FIB for the present materials, despite higher voltage used for FIB milling during the intermediate steps of the process.

After optimization of the specimen preparation method, the conditions for TEM analysis need to be considered, including the choice of microscope accelerating voltage. Figures 2(c) and (d) show two TEM images of the same region of $CH_3NH_3PbI_3$ before and after analysis at 200 kV. The area analyzed (marked with a red rectangle) suffered clear beam damage during TEM examination. Radiolysis and knock-on damage are the two most significant interactions between an incident electron beam and a specimen in the TEM. In general, radiolysis is reduced at higher accelerating voltages, whereas knock-on damage is increased [43]. Damage to the specimen depends on the nature of the material. Radiolysis remains a major limitation when studying certain ceramics and minerals and most polymers [44]. In contrast, knock-on damage usually has a stronger effect on materials such as certain semiconductors and low-Z metals/alloys [44]. Similar materials may behave differently. For example, the threshold energy required to produce a Frenkel defect by knock-on damage is smaller for Ge than for Si [45]. Our results suggest that the use of a high accelerating voltage is not appropriate for TEM studies of $CH_3NH_3PbI_3$ perovskites, as displacement damage seems to be significant. We therefore analyzed this specimen at a lower accelerating voltage of 80 kV. Figures 2(e) and (f) show TEM images of the same region of the $CH_3NH_3PbI_3$ perovskite before and after examination at 80 kV. The large and rapid damage to the material that occurred during the electron irradiation at 200 kV is no longer observed at 80 kV, demonstrating that the accelerating voltage has to be chosen carefully to avoid degradation of $CH_3NH_3PbI_3$ perovskite film. In the literature, the use of accelerating voltages of 100 kV [44–46] and 60 kV [47] and short exposure times [48] has been reported for the study of $CH_3NH_3PbI_3$ perovskites.

Figure 3(a) shows a scanning electron microscopy (SEM) image of a $CH_3NH_3PbI_3$ lamella, in which different layers of the sample structure can be observed, recorded in the FIB workstation after specimen preparation. EDX spectroscopy was used to identify the layers (see inset). The perovskite layer does not have a uniform thickness because the layers are formed from the crystallization of grains that grow independently with different orientations and sizes. It has been reported that the one-step synthesis-deposition method that was used in the fabrication of the material is affected by an imbalance between nucleation and growth rates, leading to different morphologies of the perovskite layer [49]. A DMF intermediate was used during fabrication, as it has been reported to produce an enhancement [49] that contributes to control of the crystallization of the perovskite layer [50]. However, even after using the DMF intermediate, our results indicate that the layer thickness is not uniform. In order to investigate the initial steps of layer formation, a second sample, in which the concentration of the precursor in solution was four times lower, was analyzed.

Figure 3(b) shows an SEM image of the resulting structure, in which the perovskite has not crystallized in a uniform layer, but as islands of thickness 80–100 nm. The layer shows irregular growth from the initial steps of material deposition. As shown in the regions marked by squares, the initial perovskite layer is not always flat, but contains some uneven regions, which will affect the geometry of the material when a full layer is grown. The analysis allows the adherence of the perovskite to the substrate, which is essential to obtain good performance of the solar cells [49–51], to be assessed. A second inset to figure 3(a) contains a HRTEM image of the interface between the TiO_2 and $CH_3NH_3PbI_3$. There is no gap between the materials, demonstrating good adhesion of the active layer to the TiO_2. The PMMA layer shows perfect coverage of the semiconductor in figures 3(a) and (b), suggesting that it can act as an effective protective layer for the perovskite against atmospheric conditions that could result in premature degradation.

HRTEM analysis of the perovskite layer was carried out to study the crystal structure and quality of the sample in more detail. Figure 3(c) shows a HRTEM image of the $CH_3NH_3PbI_3$ layer in figure 3(a). The layer is formed from small crystallites, whose sizes range between 5 and 20 nm. Some of the crystallites are faceted, as shown in the two insets to figure 3(c). The presence of facets in the $CH_3NH_3PbI_3$ perovskite have been observed previously [52] and results from the minimization of total surface free energy according to thermodynamic theory [52–53]. FFTs of the HRTEM images were analyzed to identify the crystal structure of the $CH_3NH_3PbI_3$ perovskite. For comparative purposes, kinematic digital diffraction patterns (DDPs) of the three possible crystalline structures of $CH_3NH_3PbI_3$ (orthorhombic (*Pnma*), tetragonal (*I4/mcm*) and cubic (*Pm3m*)) were simulated using *Eje Z* software [38]. Distances and angles were measured from the experimental FFTs automatically in *Digital Micrograph* using the script *diftool,* which provides better precision than manual measurements. Figure 3(d) shows an experimental FFT obtained from a HRTEM image of the specimen, alongside a calculated DDP for the tetragonal crystalline structure. There is a good agreement between the patterns. The angles and distances measured from the FFT were introduced into the software, which compares the measured values with all of the possibilities for the three crystal structures. This analysis is consistent with a tetragonal crystal structure of the analyzed perovskite. It was carried out in several regions of the perovskite layer, as well as in the sample with a reduced precursor concentration, showing the same result. The results of the analysis are consistent with the PL measurements, which also suggest a tetragonal crystal structure. Although some previous studies have reported that the tetragonal structure of $CH_3NH_3PbI_3$ forms at room temperature and the cubic phase forms at higher temperature (>54 °C) [54], others report that the two structures can coexist at room temperature [55]. The transition from a tetragonal to a cubic structure is accompanied by a slight distortion of PbI_6 octahedra about the *c* axis [54]. The crystal structure of the perovskites is important to understand their optical properties, as it has an effect, for example, on their band gap, with a difference of 0.03 eV reported between the band gaps of tetragonal and cubic $CH_3NH_3PbI_3$ [56].

Perovskite $CsPbBr_3$ NPs were also analyzed. Figure 4(a) shows a low magnification high-angle annular dark-field (HAADF) (S)TEM image of $CsPbBr_3$ NPs deposited on a Si substrate. The deposited perovskite particles are rectangular, with a size of $\sim 17 \pm 6$ nm. Unlike for the $CH_3NH_3PbI_3$ layers, the fabrication process involved two steps. First, the perovskite material was synthesized in a colloidal solution and deposited onto the substrate. The synthetized material in solution was analyzed by TEM before deposition onto the substrate. $CsPbBr_3$ NPs synthesized at room temperature have rectangular shapes, and similar dimensions [20]. The sizes and shapes of the $CsPbBr_3$ particles are key to control the optical properties of the material [40], [57], [58], and can be tuned by modifying the solvent, ligand and reaction time [59]. We find that these characteristics of the $CsPbBr_3$ particles are not modified after their deposition onto a solid substrate, which is encouraging for their integration into solid state devices. In the film, the particles are deposited close to each other. However, some gaps can be observed between them. Subsequent particles are deposited on the initial ones, but do not seem to fill the small gaps. The PMMA layer shows perfect coverage of the perovskite particles (see figure 4(a)), just as for the $CH_3NH_3PbI_3$ sample.

The NPs have crystalline structures, as can be observed in the inset to figure 4(a). The crystal structure was studied using the procedure described above. In this case, the three possible structures of the $CsPbBr_3$ perovskite are cubic (*Pm3m*), tetragonal (*P4/mbm*) and orthorhombic (*Pnma*). Figure 4(b) shows an FFT of the image in the inset to figure 4(a), alongside a calculated DDP for a cubic structure. Good agreement is observed, suggesting that the crystal structure of the perovskite material analyzed is cubic and consistent with the results obtained from the PL study. This cubic structure has been reported to be advantageous for $CsPbBr_3$ perovskites for photovoltaic applications due to its optimal band gap of $\sim$2.4 eV [60] in NP form. Other low temperature synthesis methods lead to yellow and non-luminescent nanocrystals, as a result of poor crystallinity or the formation of an orthorhombic crystal structure [61]. However, it has been reported that the cubic structure suffers a transformation to the orthorhombic structure when it is exposed to ambient conditions [62]. Several options have been considered to stabilize the cubic structure. For example, purification with methyl acetate has proved to be a route to stabilize the cubic structure under ambient conditions for months [63]. The introduction of a layer of PMMA is also a potential solution, as it provides efficient coverage of the perovskite, as shown in the present work.

In order to study the compositional distribution in the perovskite layer, EDX analysis of the particles was carried out, as shown in figures 4(c) and (d). The EDX map shown in figure 4(c) confirms the expected uniform distribution of the elements. The slight increase in signal on the left side of the particle is thought to result from an increase in the thickness of the material in this region, as it is found for all of the elements. In figure 4(d), although the distribution of Br and

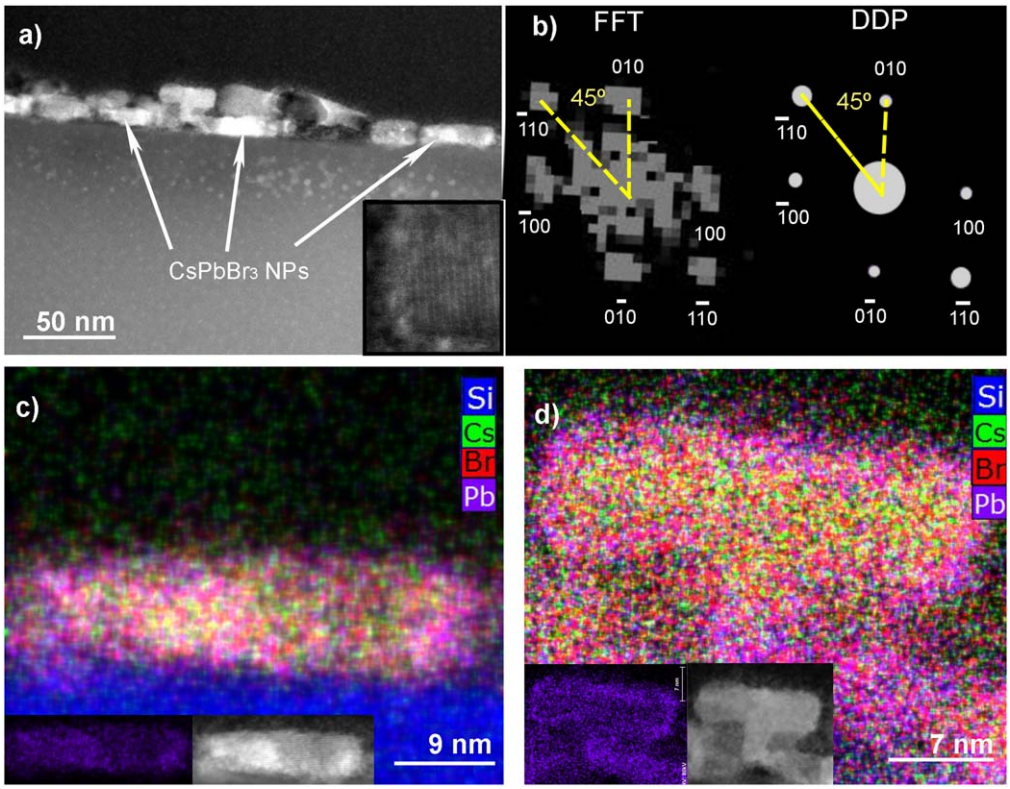

Figure 4. (a) Low magnification HAADF (S)TEM image of $CsPbBr_3$ NPs deposited on Si, with the inset showing a high-resolution HAADF (S)TEM image of one of the $CsPbBr_3$ particles. (b) Experimental FFT of the image in the inset to (a) shown alongside a DDP calculated for a cubic structure. (c) and (d) EDX maps of $CsPbBr_3$ NPs. Inset showing the Pb distributions and HAADF (S)TEM images.

Cs is uniform, the distribution of Pb is inhomogeneous. Pb^0 formation in halide perovskites under light illumination has been previously reported using XPS and XRD [64]. The EDX map shows a larger amount of Pb at the edges of the NP. An inset showing only the Pb distribution is included to show the enriched edges. Similar results were found in some other $CsPbBr_3$ NPs in this sample, although with a lower degree of segregation. Recent studies reported the degradation of hybrid and all-inorganic lead halide perovskites under electron beam irradiation in the TEM [33]. In particular, it was reported that $CsPbBr_3$ particles undergo a radiolysis process that results in the desorption of Br atoms and the reduction of Pb^{2+} ions to Pb^0 [33], which diffuse and aggregate to form non-epitaxial Pb crystals [33]. The damage was found to be particularly pronounced at the corners and edges of the perovskite layer, as there is a lower diffusion barrier for Pb^0 in these regions [33]. Our results also point in this direction. The longer exposure times used for the acquisition of EDX maps in the electron microscope, in comparison to conventional imaging modes, results in the initial stages of material decomposition in some particles. As mentioned above, the damage of the $CsPbBr_3$ perovskites under the electron beam consists on the reduction of Pb^{+2}–Pb^0 and then the diffusion of Pb atoms to form Pb particles. The diffusion of Pb atoms is a procedure that needs time. When the exposure time is short, only a small amount of Pb^{+2} is reduced to Pb and there is not much time for the Pb diffusion. However, when the exposure time is longer as during the acquisition of EDX spectra, a larger amount of Pb^{+2} is reduced and diffuses to form Pb aggregates. The observed decomposition is more pronounced at the edges of the particles, as shown in figure 4(d). The edge of a material (as well as any other defected region) is a part of the material easier to be modified as the atoms do not have all their bonds completed, therefore initial Pb particles would be expected to be formed in this region, as shown previously by [33, 65, 66]. Also, the diffusion barrier is lower in this region, therefore some accumulation is expected to be found at the edge of the particles. Care is therefore required in the study of perovskite materials using (S)TEM techniques, in order to avoid degradation of the material and to obtain reliable results.

Conclusions

We have shown that specimen preparation using FIB milling instead of conventional techniques and the use of a low accelerating voltage of 80 kV are required for (S)TEM analysis of $APbX_3$ perovskites in order to avoid degradation of the material on both standard thin films and layers formed by NPs. Analysis of $CH_3NH_3PbI_3$ synthesized by a one-step method shows that the active layer grows irregularly on a Si substrate from the initial steps of the crystallization process, with good adherence to a TiO_2 layer. The crystal structure of the $CH_3NH_3PbI_3$ perovskite is shown to be tetragonal. A sharp absorption edge is localized at 750–760 nm, while the

exciton absorption resonance is centered at 750 nm. $CsPbBr_3$ NPs deposited on a substrate are shown to have parallelepipedal shapes similar to those before the deposition process. Their crystal structure is cubic with a PL line centered at 517 nm with a FWHM of 21 nm, which is optimal for light-emitting diodes and displays with high color rendering. Despite the low voltage used for (S)TEM analysis, long irradiation times result in segregation of Pb to the edges of the NPs, which is the first step towards decomposition of the material. The analysis highlights the care that is needed for (S)TEM measurements of both bulk and NP perovskite thin films.

Acknowledgments

This work was supported by the Spanish MINECO (projects TEC2014-53727-C2-1-R, -2-R and TEC2017-86102-C2-2-R) and Junta de Andalucía (PAI research group TEP-946). The research leading to these results has received co-funding from the European Union. BCH is grateful for the support of the National Council of Technological and Scientific Development (CNPq), Brazil, through the Science without Borders program.

ORCID iDs

N Fernández-Delgado https://orcid.org/0000-0002-6295-2475
M Luysberg https://orcid.org/0000-0002-5613-7570

References

[1] Kalaiselvi C R, Muthukumarasamy N, Velauthapillai D, Kang M and Senthil T S 2018 Importance of halide perovskites for next generation solar cells-a review *Mater. Lett.* **219** 198–200
[2] Liu X, Xu T, Li Y, Zang Z, Peng X, Wei H, Zha W and Wang F 2018 Enhanced x-ray photon response in solution-synthesized $CsPbBr_3$ nanoparticles wrapped by reduced graphene oxide *Sol. Energy Mater. Sol. Cells* **187** 249–54
[3] Wang M, Zang Z, Yang B, Hu X, Sun K and Sun L 2018 Performance improvement of perovskite solar cells through enhanced hole extraction: the role of iodide concentration gradient *Sol. Energy Mater. Sol. Cells* **185** 117–23
[4] Li C, Zang Z, Chen W, Hu Z, Tang X, Hu W, Sun K, Liu X and Chen W 2016 Highly pure green light emission of perovskite $CsPbBr_3$ quantum dots and their application for green light-emitting diodes *Opt. Express* **24** 54109–14
[5] Zhang L *et al* 2017 Ultra-bright and highly efficient inorganic based perovskite light-emitting diodes *Nat. Commun.* **8** 1–8
[6] Li C, Zang Z, Han C, Hu Z, Tang X, Du J, Leng Y and Sun K 2017 Enhanced random lasing emission from highly compact $CsPbBr_3$perovskite thin films decorated by ZnO nanoparticles *Nano Energy* **40** 195–202
[7] Wang Y, Li X, Nalla V, Zeng H and Sun H 2017 Solution-processed low threshold vertical cavity surface emitting lasers from all-linorganic perovskite nanocrystals *Adv. Funct. Mater.* **27** 1605088
[8] Sutherland B R and Sargent E H 2016 Perovskite photonic sources *Nat. Photon.* **10** 295–302
[9] de Wolf S, Holovsky J, moon S-J, Löper P, Niesen B, Ledinsky M, Haug F, Yum J and Ballif C 2014 Organometallic halide perovskites: sharp optical absorption edge and its relation to photovoltaic performance *J. Phys. Chem.* C **5** 1035–139
[10] Kim H S *et al* 2012 Lead iodide perovskite sensitized all-solid-state submicron thin film mesoscopic solar cell with efficiency exceeding 9% *Sci. Rep.* **2** 1–7
[11] (https://nrel.gov/pv/assets/images/efficiency-chart.png)(n.d.)
[12] Suárez I, Juárez-Pérez E J, Bisquert J, Mora-Serõ I and Martínez-Pastor J P 2015 Polymer/perovskite amplifying waveguides for active hybrid silicon photonics *Adv. Mater.* **27** 6157–62
[13] Eperon G E, Habisreutinger S N, Leijtens T, Bruijnaers B J, van Franeker J J, deQuilettes D W, Pathak S, Sutton R J, Grancini G and Ginger D S 2015 The importance of moisture in hybrid lead halide perovskite thin film fabrication *ACS Nano* **9** 851–9380
[14] Troughton J, Hooper K and Watson T M 2017 Humidity resistant fabrication of $CH_3NH_3PbI_3$ perovskite solar cells and modules *Nano Energy* **39** 60–8
[15] Kulbak M, Gupta S, Kedem N, Levine I, Bendikov T, Hodes G and Cahen D 2016 Cesium enhances long-term stability of lead bromide perovskite-based solar cells *J. Phys. Chem. Lett.* **7** 167–72
[16] Fabregat-Santiago F, Kulbak M, Zohar A, Vallés-Pelarda M, Hodes G, Cahen D and Mora-Seró I 2017 Deleterious effect of negative capacitance on the performance of halide perovskite solar cells *ACS Energy Lett.* **2** 2007–13
[17] Swarnkar A, Chulliyil R, Ravi V K, Irfanullah M, Chowdhury A and Nag A 2015 Colloidal $CsPbBr_3$ perovskite nanocrystals: luminescence beyond traditional quantum dots *Angew. Chem.* **127** 15644–8
[18] Li X, Wu Y, Zhang S, Cai B, Gu Y, Song J and Zeng H 2016 $CsPbX_3$ quantum dots for lighting and displays: room-temperature synthesis, photoluminescence superiorities, underlying origins and white light-emitting diodes *Adv. Funct. Mater.* **26** 2435–45
[19] Stoumpos C C *et al* 2018 Crystal growth of the perovskite semiconductor $CsPbBr_3$: a new material for high-energy radiation detection *Cryst. Growth Des.* **13** 2722–7
[20] Clasen Hames B, Sánchez Sánchez R, Fakharuddin A and Mora-Seró I 2018 A comparative study of light-emitting diodes based on all-inorganic perovskite nanoparticles ($CsPbBr_3$) synthesized at room temperature and by a hot-injection method *ChemPlusChem* **83** 1–7
[21] Ding J, Du S, Zuo Z, Zhao Y, Cui H and Zhan X 2017 High detectivity and rapid response in perovskite $CsPbBr_3$ single-crystal photodetector *J. Phys. Chem.* C **121** 4917–23
[22] Hoffman J B, Zaiats G, Wappes I and Kamat P V 2017 $CsPbBr_3$ solar cells: controlled film growth through layer-by-layer quantum dot deposition *Chem. Mater.* **29** 9767–74
[23] Wagner L, Mundt L E, Mathiazhagan G, Mundus M, Schubert M C, Mastroianni S, Würfel U, Hinsch A and Glunz S W 2017 Distinguishing crystallization stages and their influence on quantum efficiency during perovskite solar cell formation in real-time *Sci. Rep.* **7** 1–6
[24] Ghosh D, Ali M Y, Chaudhary D K and Bhattacharyya S 2018 Dependence of halide composition on the stability of highly efficient all-inorganic cesium lead halide perovskite quantum dot solar cells *Sol. Energy Mater. Sol. Cells* **185** 28–35
[25] Uratani H and Yamashita K 2017 Charge carrier trapping at surface defects of perovskite solar cell absorbers: a first-principles study *J. Phys. Chem. Lett.* **8** 742–6

[26] Yang Y, Yang M, Moore D T, Yan Y, Miller E M, Zhu K and Beard M C 2017 Top and bottom surfaces limit carrier lifetime in lead iodide perovskite films *Nat. Energy* **2** 1–7

[27] Yang W S, Noh J H, Jeon N J, Kim Y C, Ryu S, Seo J and Seok S I 2015 High-performance photovoltaic perovskite layers fabricated through intramolecular exchange *Science* **348** 1234–7

[28] Sharenko A and Toney M F 2016 Relationships between lead halide perovskite thin-film fabrication, morphology, and performance in solar cells *J. Am. Chem. Soc.* **138** 463–70

[29] Messegee Z, Mamun A, Ava T T, Namkoong G and Abdel-fattah T M 2018 Characterization of perovskite ($CH_3NH_3PbI_3$) degradation with the integration of different polymers for increased stability *Mater. Lett.* **236** 159–62

[30] Li X, Xue Z, Luo D, Huang C, Liu L, Qiao X and Liu C 2018 A stable lead halide perovskite nanocrystals protected by PMMA *Sci. China Mater.* **61** 363–70

[31] Meggiolaro D, Motti S, Mosconi E, barker A, Ball J, Perini C A R, Deschler F, Petrozza A and Angelis F D 2018 Iodine chemistry determines the defect tolerance of lead-halide perovskites *Energy Environ. Sci.* **11** 702–13

[32] Vassilakopoulou A, Papadatos D and Koutselas I 2017 Light emitting diodes based on blends of quasi-2D lead halide perovskites stabilized within mesoporous silica matrix *Microporous Mesoporous Mater.* **249** 165–75

[33] Dang Z, Shamsi J, Palazon F, Imran M, Akkerman Q A, Park S, Bertoni G, Prato M, Brescia R and Manna L 2017 *In situ* transmission electron microscopy study of electron beam-induced transformations in colloidal cesium lead halide perovskite nanocrystals *ACS Nano* **11** 2124–32

[34] Xiao M *et al* 2014 Procedure for highly efficient lead (supporting) *Angew. Chem.* **126** 10056–61

[35] Jeangros Q, Duchamp M, Werner J, Kruth M, Dunin-Borkowski R E, Niesen B, Ballif C and Hessler-Wyser A 2016 *In situ* TEM analysis of organic-inorganic metal-halide perovskite solar cells under electrical bias *Nano Lett.* **16** 7013–8

[36] Zhang M, Li H, Jing Q, Lu Z and Wang P 2017 Atomic characterization of byproduct nanoparticles on cesium lead halide nanocrystals using high-resolution scanning transmission electron microscopy *Crystals* **8** 1–10

[37] Suárez I, Larrue A, Rodríguez-Cantó P J, Almuneau G, Abargues R, Chirvony V S and Martínez-Pastor J P 2014 Efficient excitation of photoluminescence in a two-dimensional waveguide consisting of a quantum dot-polymer sandwich-type structure *Opt. Lett.* **39** 4962

[38] Pérez-Omil J A 2016 Eje Z, University of Cadiz

[39] Herz L M 2016 Charge-carrier dynamics in organic–inorganic metal halide perovskites *Annu. Rev. Phys. Chem.* **67** 65–89

[40] Protesescu L, Yakunin S, Bodnarchuk M I, Krieg F, Caputo R, Hendon C H, Yang R X, Walsh A and Kovalenko M V 2015 Nanocrystals of cesium lead halide perovskites ($CsPbX_3$, X = Cl, Br, and I): novel optoelectronic materials showing bright emission with wide color gamut *Nano Lett.* **15** 3692–6

[41] Tang X *et al* 2016 Room temperature single-photon emission and lasing for all-inorganic colloidal perovskite quantum dots *Nano Energy* **28** 462–8

[42] Raja S N, Bekenstein Y, Koc M A, Fischer S, Zhang D, Lin L, Ritchie R O, Yang P and Alivisatos A P 2016 Encapsulation of perovskite nanocrystals into macroscale polymer matrices: enhanced stability and polarization *ACS Appl. Mater. Interfaces* **8** 35523–33

[43] Egerton R F, Li P and Malac M 2004 Radiation damage in the TEM and SEM *Micron* **35** 399–409

[44] Williams D B and Carter C B 2009 *Transmission Electron Microscopy* (New York: Springer)

[45] Pepinsky V and Hoshino O 1958 Radiation damage in Ge and Si detected by carrier lifetime changes: damage thresholds *Phys. Rev.* **111** 432–9

[46] Zhong D, Cai B, Wang X, Yang Z, Xing Y, Miao S, Zhang W H and Li C 2015 Synthesis of oriented TiO_2 nanocones with fast charge transfer for perovskite solar cells *Nano Energy* **11** 409–18

[47] Ha S-T, Su R, Xing J, Zhang Q and Xiong Q 2017 Metal halide perovskite nanomaterials: synthesis and applications *Chem. Sci.* **8** 2522–36

[48] Zhou Y, Vasiliev A L, Wu W, Yang M, Pang S, Zhu K and Padture N P 2015 Crystal morphologies of organolead trihalide in mesoscopic/planar perovskite solar cells *J. Phys. Chem. Lett.* **6** 2292–7

[49] Yao Z, Jones T W, Grigore M, Duffy N W, Anderson K F, Dunbar R B, Feron K, Hao F, Lin H and Wilson G J 2018 Tunable crystallization and nucleation of planar $CH_3NH_3PbI_3$ through solvent-modified interdiffusion *ACS Appl. Mater. Interfaces* **10** 14673–83

[50] Li W, Fan J, Li J, Mai Y and Wang L 2015 Controllable grain morphology of perovskite absorber film by molecular self-assembly toward efficient solar cell exceeding 17% *J. Am. Chem. Soc.* **137** 10399–405

[51] Shao J, Yang S and Liu Y 2017 Efficient bulk heterojunction $CH_3NH_3PbI_3$-TiO_2 solar cells with TiO_2 nanoparticles at grain boundaries of perovskite by multi-cycle-coating strategy *ACS Appl. Mater. Interfaces* **9** 16202–14

[52] Chen Y, Yang S, Chen X, Zheng Y C, Hou Y, Li Y H, Zeng H D and Yang H G 2015 Direct insight into crystallization and stability of hybrid perovskite $CH_3NH_3PbI_3$ via solvothermal synthesis *J. Mater. Chem.* A **3** 15854–7

[53] Wang Y Q, Bin Xu S, Deng J G and Gao L Z 2017 Enhancing the efficiency of planar heterojunction perovskite solar cells via interfacial engineering with 3-aminopropyl trimethoxy silane hydrolysate *R. Soc. Open Sci.* **4** 170980

[54] Poglitsch A and Weber D 1987 Dynamic disorder in methylammoniumtrihalogenoplumbates (II) observed by millimeter-wave spectroscopy *J. Chem. Phys.* **87** 6373–8

[55] Kim T W *et al* 2018 Self-organized superlattice and phase coexistence inside thin film organometal halide perovskite *Adv. Mater.* **30** 1–8

[56] Tao S X, Cao X and Bobbert P A 2017 Accurate and efficient band gap predictions of metal halide perovskites using the DFT-1/2 method: GW accuracy with DFT expense *Sci. Rep.* **7** 1–39

[57] Shinde A, Gahlaut R and Mahamuni S 2017 Low-temperature photoluminescence studies of $CsPbBr_3$ quantum dots *J. Phys. Chem.* C **121** 14872–8

[58] Ye S, Zhao M, Song J and Qu J 2018 Controllable emission bands and morphologies of high-quality $CsPbX_3$ perovskite nanocrystals prepared in octane *Nano Res.* 1–10

[59] Seth S and Samanta A 2016 A facile methodology for engineering the morphology of $CsPbX_3$ perovskite nanocrystals under ambient condition *Sci. Rep.* **6** 1–7

[60] De Jong E M L D, Yamashita G, Gomez L, Ashida M, Fujiwara Y and Gregorkiewicz T 2017 Multiexciton lifetime in all-inorganic $CsPbBr_3$ perovskite nanocrystals *J. Phys. Chem.* C **121** 1941–7

[61] Aceves R, Babin V, Barboza Flores M, Fabeni P, Nikl M, Nitsch K, Pazzi G P, Perez Salas R and Zazubovich S 2001 Luminescence of $CsPbCl_3$-like quantum dots in CsCl:Pb crystals *Phys. Status Solidi* **225** 247–55

[62] Beal R E, Slotcavage D J, Leijtens T, Bowring A R, Belisle R A, Nguyen W H, Burkhard G F, Hoke E T and McGehee M D 2016 Cesium lead halide perovskites with improved stability for tandem solar cells *J. Phys. Chem. Lett.* **7** 746–51

[63] Swarnkar A, Marshall A R, Sanehira E M, Chernomordik B D, Moore D T, Christians J A, Chakrabarti T and Luther J M 2016 Quantum dot-induced phase stabilization of α-$CsPbI_3$ perovskite for high-efficiency photovoltaics *Science* **354** 92–5

[64] Juarez-Perez E J, Ono L K, Maeda M, Jiang Y, Hawash Z and Qi Y 2018 Photodecomposition and thermal decomposition in methylammonium halide lead perovskites and inferred design principles to increase photovoltaic device stability *J. Mater. Chem.* A **6** 9604–12

[65] Dou L, Wong A B, Yu Y, Lai M, Kornienko N, Ginsberg N S, Wang L, Alivisatos A P and Yang P 2015 Atomically thin two-dimensional organic–inorganic hybrid perovskites *Res. Rep.* **349** 1518–21

[66] Akkerman Q A *et al* 2016 Solution synthesis approach to colloidal cesium lead halide *J. Am. Chem. Soc.* **138** 1010–6